ECS Transactions, 3(7)45-54(2006)
10.1149/1.2355793, copyright The Electrochemical Society

Low-Field Electron Mobility in Stressed UTB SOI MOSFETs for Different Substrate Orientations

E. Ungersboeck, V. Sverdlov, H. Kosina, and S. Selberherr

Institute for Microelectronics, TU Wien, Gusshausstr. 27–29, 1040 Wien, Austria

To continue improvement of CMOS device performance process induced uniaxial stress is widely adopted in logic technologies starting from the 90 nm technology generation. In this work we model stress induced electron mobility enhancement in bulk Si, inversion layers formed on (001) and (110) substrate orientations, and UTB MOSFETs using the Monte Carlo method. Uniaxial stress effects on the bulk band structure are incorporated by adapting the non-local empirical pseudopotential method with spin-orbit interaction for arbitrary strain conditions. Stress induced change of the electron effective mass is found to be very important to enhance mobility in UTB MOSFETs. Simulation results of electron mobility are compared to experimental data and good qualitative agreement is found.

Introduction

With ongoing scaling of MOSFETs the semiconductor industry is facing several critical challenges. Among them are the high gate leakage current for very thin gate dielectrics, the difficulty to maintain a high I_{on}/I_{off} ratio, short channel effects, and the high power dissipation for small transistors. Many innovations are needed to circumvent these problems, and various new materials and architectures are under investigation. Strain engineering will certainly maintain its importance, as it improves transistor performance even at aggressively scaled channel lengths by fundamentally altering the band structure of semiconductors.

Theoretical modeling of strain induced mobility enhancement for electrons and holes is an important issue with some critical questions still open (1, 2). In particular, due to the uncertainty in the scattering models and parameters for the inversion layer in conjunction with the arising numerical complexity, one is forced to do severe approximations. For this reason a phenomenological approach based on the empirically measured piezoresistance coefficients is often used by industry to predict mobility enhancement for electrons and holes. With this approach, the effect of stress on the mobilities in MOSFETs is estimated using bulk- or inversion-layer piezoresistance coefficients (3). A disadvantage of this approach is that the validity of the piezoresistance coefficients is restricted to small strains and stresses ($< 500\,\mathrm{MPa}$), even though much higher values can be reached in current technologies.

In this work we analyze electron mobility enhancement by solving the Boltzmann equation using a MC method. Under small stress the model is validated against the approach with piezoresistance coefficients. The importance of accurate band structure modeling to explain experimentally observed mobility enhancement is highlighted. For this purpose the band structure of arbitrarily strained Si was calculated using the non-local empirical pseudopotential method (EPM). We present simulation results for mobility enhancement in bulk Si and for Si inversion layers with one and two interfaces, being formed in ultra thin body MOSFETs.

Stress Effect on Band Structure

Strain induced electron mobility enhancement ($\Delta\mu$) is frequently described on the basis of linear deformation potential theory (4). According to this theory strain induces a shift of the band energy minima, potentially lifting the degeneracy of the conduction band valleys, whereas any strain induced electron mass change is neglected (5). However, it was shown recently that stress along $\langle 110 \rangle$ leads to a significant effective mass change of the Δ_2 band minima (6). We performed band structure calculations adapting the empirical pseudopotential method for general strain conditions (7) and obtain results similar to (6) for stress along $\langle 110 \rangle$.

Novel stress engineering techniques like uniaxial-biaxial stress hybridization have been reported, that allow the generation of various stress patterns in the transistor channel (8). In Fig. 1 we show that an even more pronounced effective mass change occurs in systems with in-plane tensile uniaxial [110] stress parallel to the channel in [110] and in-plane uniaxial compressive [$\bar{1}$10] stress perpendicular to the channel. A peculiarity of this stress configuration is, that only small valley splitting occurs, as the strain tensor resulting from this stress configuration has vanishing diagonal elements. Fig. 1 also shows the effective mass change in a system with biaxial tensile in-plane stress. Our simulation results suggest that the effective mass change is small for this kind of stress. An effective mass change is observed, whenever the strain tensor in the crystal system contains off-diagonal components. If stress is applied along $\langle 100 \rangle$, or when Si is epitaxially grown on {001}-oriented SiGe, the strain tensor is diagonal and the effective mass change is comparatively small.

Stress Induced Mobility Enhancement

The effect of stress on the bulk mobility and the inversion layer mobility is expected to be different, if we assume that mobility enhancement is predominately a result of a stress induced band structure change. This is also reflected in different piezoresistance coefficients for bulk and inversion layers (3). In quantum confined systems each conduction band minimum splits into a set of subbands. Depending of the sign and direction of applied stress, the intrinsic splitting between the subband ladders can be increased or decreased. In the following it will be shown that, in order to gain a

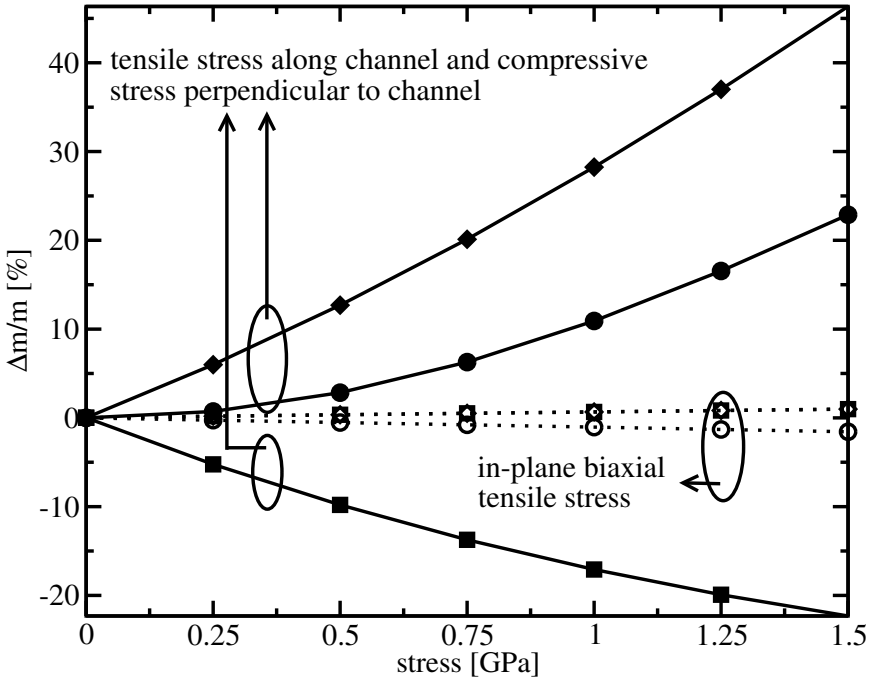

Fig. 1: Relative effective mass change of the [001] X-valley under combined uniaxial tensile stress along [110] and uniaxial compressive stress along $[\bar{1}10]$ (solid lines) and biaxial tensile stress (dotted lines). The mass change is plotted along $[\bar{1}10]$ (diamonds), [001] (circles), and [110] (squares).

better understanding of stress induced mobility enhancement in UTB-MOSFETs, it is illustrative to first study stress effects on the bulk mobility.

Bulk

The Monte Carlo simulator VMC (9) allows the simulation of carrier transport in arbitrarily strained Si and SiGe. It was demonstrated that the bulk mobility enhancement occurring in strained $Si_{1-x}Ge_x$ layers on $Si_{1-y}Ge_y$ substrates for arbitrary substrate orientations can be accurately reproduced (10). Recent extensions consider strain effects arising from uniaxial stress. We start the discussion with an analysis of the effect of [110] tensile stress on the electron mobility in the (001) plane, as this stress condition is commonly used in strain engineered n-channel MOSFETs. Fig. 2 shows the constant energy surfaces of the conduction band in unstrained Si located along the six equivalent $\langle 100 \rangle$ directions. In the unstrained crystal the six valleys are equally populated, resulting in an isotropic mobility. If uniaxial tensile stress is applied along [110], experimentally an anisotropic mobility enhancement in the (001) plane was observed (11, 15), which is also reflected in the linear piezoresistance coefficients, yielding the most pronounced mobility enhancement parallel to the stress direction. Only when the effective mass change of the out-of-plane valleys is introduced in the simulation, the numerical model can reproduce the anisotropic mobility enhancement. For small stress good agreement with the enhancement predicted from the piezoresistance coefficients is found (Fig. 2).

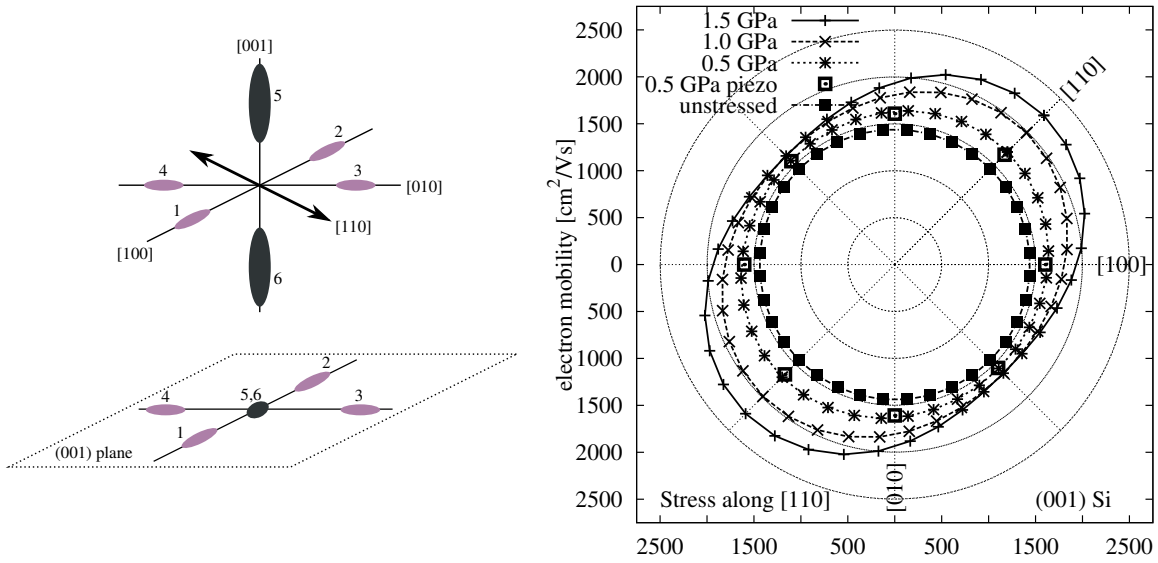

Fig. 2: Left: Constant energy surfaces of the Si conduction band under uniaxial tensile stress along [110] with projection on the (001) plane. Right: Simulated in-plane electron mobility for various stress levels. At 500 MPa simulation results are compared to mobility calculated from the piezoresistance coefficients (open squares).

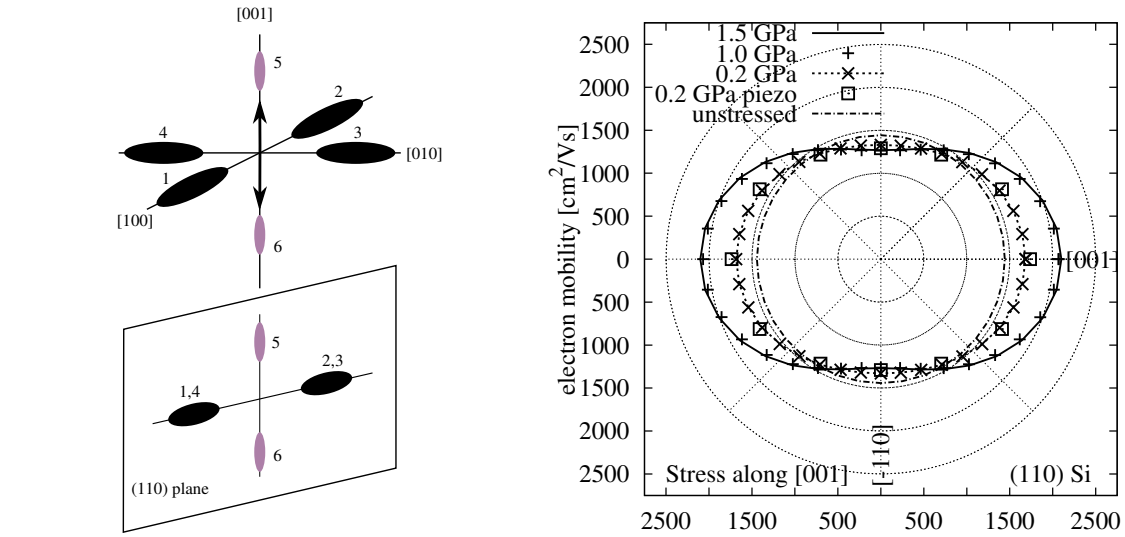

Fig. 3: Left: Constant energy surfaces of the Si conduction band under uniaxial tensile stress along [001] with projection on the (110) plane. Right: Simulated in-plane electron mobility for various stress levels. At 200 MPa simulation results are compared to mobility calculated from the piezoresistance coefficients (open squares).

We want to stress that a model based on linear deformation potential theory alone cannot reproduce the anisotropy in the (001) plane: According to this theory, the bands shift by an amount linearly related to the strain in the semiconductor, whereas the shape of the bands is not altered. Under tensile stress along [110], the out-of-plane valleys (labeled 5,6 in Fig. 2) have a higher population than the in-plane valleys (labeled 1-4) and will therefore mainly determine the mobility. Since, according to deformation potential theory, the energy dispersion in the out-of-plane valleys is isotropic in the (001) plane, isotropic mobility enhancement for this stress configuration is expected, which clearly contradicts experimental observations for large stress levels.

Next we discuss uniaxial tensile stress along [001], as this stress is favorable for electron mobility enhancement on (110) oriented substrates with channel and stress in [001] direction. Under this stress condition four valleys move down in energy (labeled 1-4 in Fig. 3). The resulting in-plane mobility is shown in Fig. 3. Similar to the (001) plane, under stress the mobility is anisotropic. The highest mobility component is observed along the [001] direction. However, band structure calculations have shown that under $\langle 100 \rangle$ stress the effective mass change is negligible. Thus, $\Delta\mu$ stems from the stress induced valley shifts only. Again, for small stress levels a similar $\Delta\mu$ can be found from the piezoresistance coefficients, validating the MC simulation results. However, it can also be seen from Fig. 3, that $\Delta\mu$ saturates as stress is increased. Models based on piezoresistance coefficients will thus overestimate $\Delta\mu$ for large stress levels.

Inversion layers formed on (001) and (110) oriented substrates

The inversion layer mobility was calculated by means of a Monte Carlo method taking into account the subband structure and phonon scattering, surface roughness scattering according to the model of Prange and Nee (13), and screening effects (14). Depending on the substrate orientation the six-fold degenerate X-valley splits into up to three different subband ladders. While on (001) substrate the subbands of the lowest subband ladder (unprimed ladder) are spherical and the ladder is two-fold degenerate, on (110) substrate the subbands are elliptical and the unprimed ladder is four-fold degenerate. The higher density of states and larger transport masses on (110) substrate yield a lower inversion layer mobility as compared to (001) substrate. This can be seen in Fig. 4, where we compare experimental data (11, 12) to simulation results.

We will continue the analysis by investigating the origin of the electron mobility enhancement of inversion layers with uniaxial stress. To demonstrate the influence of the orientation, subband Monte Carlo simulations are performed for (001) and (110) oriented substrates. It is shown that uniaxial stress leads to a pronounced anisotropy of the in-plane mobility for both substrate orientations. While on (110) substrate this effect stems from the ellipsoidal shape of the lowest subband ladder, the effective mass change induced by [110] stress explains the anisotropic mobility of [110] uniaxially stressed (001) wafers.

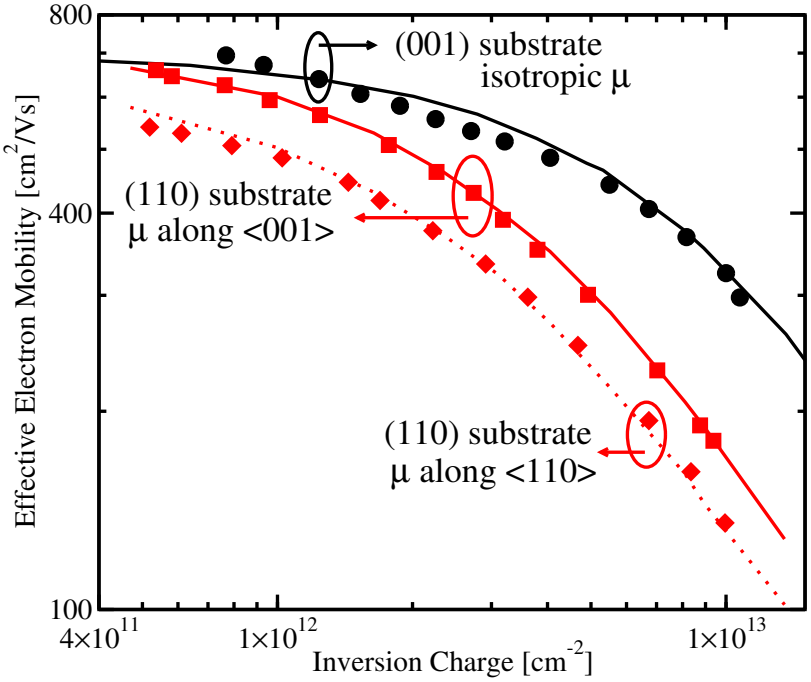

Fig. 4: Simulated μ_{eff} for substrate orientation (001) and (110) compared to measurements (11, 12) (symbols). The anisotropic μ_{eff} on the (110) substrate is given along $\langle 001 \rangle$ and $\langle 110 \rangle$.

The stress induced changes of the bulk effective mass, calculated using the EPM method, are incorporated in subband MC simulations. In Fig. 5 the mobility components parallel and perpendicular to stress direction [110] for two tensile stress levels are compared to the unstrained mobility. Tensile stress along [110] has two beneficial effects on the parallel mobility component: The splitting between the unprimed and primed ladders is increased, and the transport mass in direction of the stress is reduced with respect to the unstrained case. From these two effects one can understand the mobility enhancement parallel to the stress direction at all inversion layer densities. Perpendicular to stress, the effective mass is increased by stress, leading to a smaller mobility enhancement in this direction. Contrary to biaxially strained Si, a saturation of the mobility enhancement is not expected as the EPM simulations suggest an effective mass change roughly linearly proportional to stress.

To enhance the mobility on (110) substrate a uniaxial tensile stress along [001] is applied, as this stress condition increases the splitting between the primed and unprimed ladders. From EPM simulations we get only a negligible change of the effective masses which determine the transport in the subband ladders. From Fig. 6 we observe that stress increases the component of μ_{eff} parallel to the stress direction, whereas the perpendicular mobility is smaller compared to the unstressed case. Since no effective mass change occurs, the mobility change is expected to saturate at larger stress (~ 1 GPa), as soon as the primed ladder becomes depopulated. Our results are in good agreement with experimental data for the anisotropic mobility enhancement on (001) and (110) oriented substrates (15).

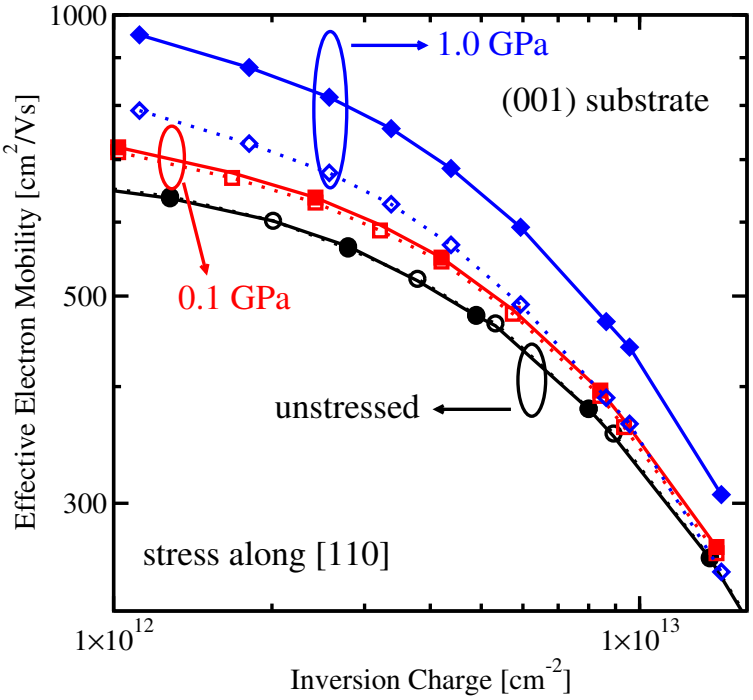

Fig. 5: Simulated component of the mobility parallel (closed symbols) and perpendicular (open symbols) to stress direction [110] with no stress (circles), 0.1 GPa (squares), and 1.0 GPa stress (diamonds).

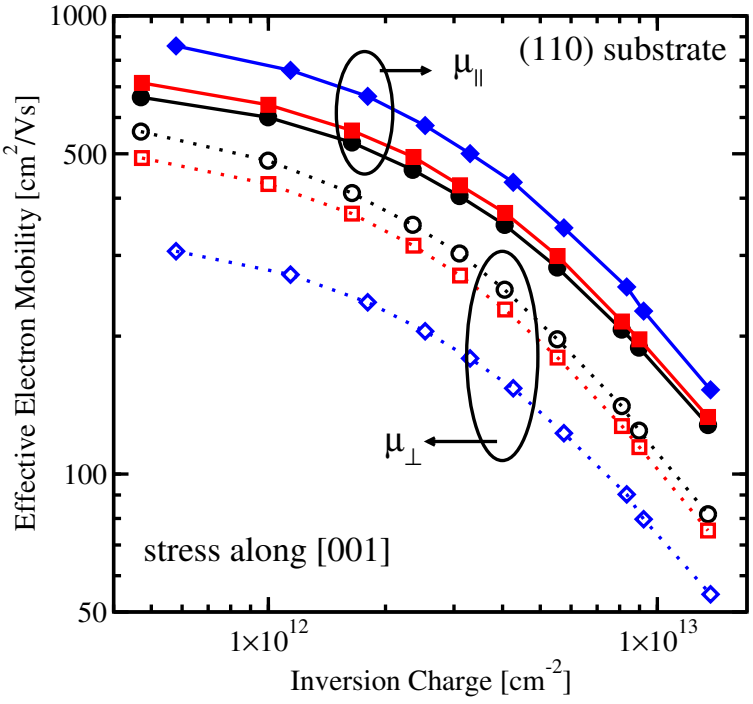

Fig. 6: Simulated component of the mobility parallel (closed symbols) and perpendicular (open symbols) to stress direction [001] with no stress (circles), 0.1 GPa (squares), and 1.0 GPa stress (diamonds).

Finally, the influence of stress on the effective electron mobility enhancement in UTB MOSFETs is analyzed. On (001) substrate we have shown that one can benefit from two effects if stress direction and channel direction are both [110], because of stress induced valley splitting and stress induced effective mass change. At relatively large body thicknesses like T_{SOI}=20 nm, $\Delta\mu_{\mathrm{eff}}$ can be understood from a combination of the two effects yielding an anisotropic μ_{eff} as compared to the unstressed system (see Fig. 7).

In ultra-thin Si bodies, however, the strong quantum confinement induces a large intrinsic valley splitting, thus the stress induced valley shifts have a negligible effect on the mobility. The larger component $\mu_{\mathrm{eff}||}$ and smaller component $\mu_{\mathrm{eff}\perp}$ parallel and perpendicular to the stress direction, respectively, at T_{SOI}=2.4 nm (compare Fig. 7) result from the effective mass change only and are found in good agreement with experimental data (6).

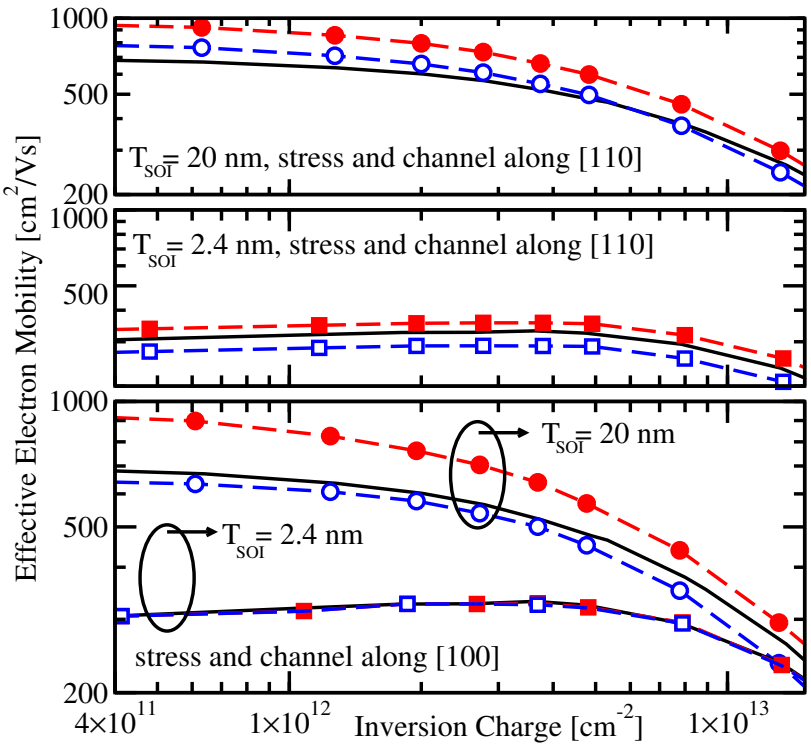

Fig. 7: Simulated effective mobility for substrate orientation (001), two channel orientations and two body thicknesses of unstressed (solid lines) and 1 GPa stressed Si (dashed lines). The mobilities are plotted parallel (closed symbols) and perpendicular (open symbols) to the stress direction.

In Fig. 7 the effect of uniaxial stress on the mobility on (001) oriented substrate with channel direction and stress direction parallel to [100] is shown. The effect of uniaxial tensile stress in the channel direction is qualitatively different from wafers with stress and channel along [110]. Stress along [100] lifts the degeneracy of the fourfold

(primed) ladder. Since no effective mass change occurs, $\Delta\mu_{\text{eff}}$ occurring at large T_{SOI} is a result of subband ladder repopulation only. As the body thickness is decreased, the population of the higher subband ladders inevitably decreases, and strain cannot further decrease the population. Therefore, in Fig. 7 no mobility enhancement is seen at $T_{\text{SOI}} = 2.4\,\text{nm}$.

Stress induced $\Delta\mu_{\text{eff}}$ on (110) oriented substrates can be understood from similar arguments. Tensile stress along [001], which increases the parallel bulk and inversion layer mobility (see Fig. 3 and Fig. 6), does not alter the mobilities at small T_{SOI}, because it does not change the effective masses, but merely increases the splitting between the primed and unprimed subband ladders. Fig. 8 shows how the stress induced mobility enhancement, observed at $T_{\text{SOI}} = 20.0\,\text{nm}$, vanishes at $T_{\text{SOI}} = 3.0\,\text{nm}$.

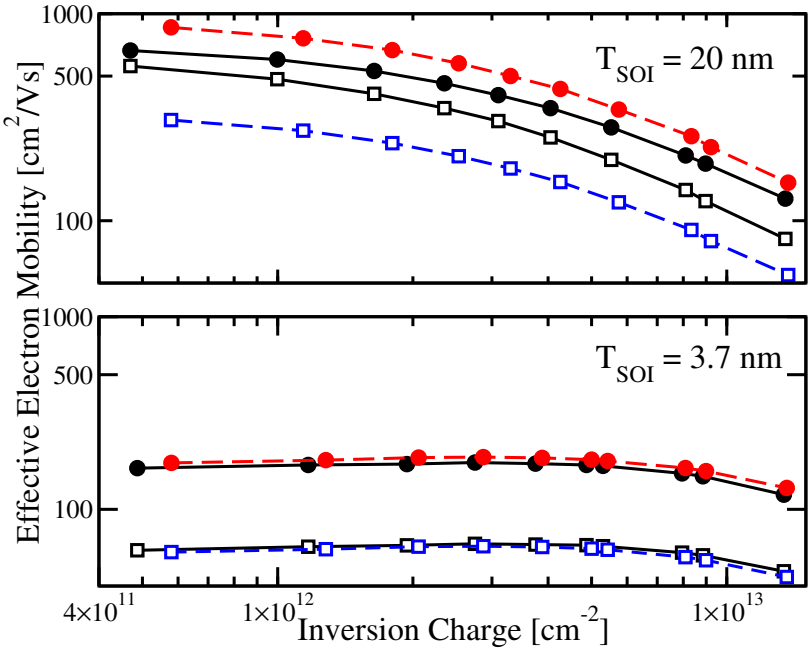

Fig. 8: Simulated effective mobility for substrate orientation (110) of unstressed (solid lines) and 1 GPa stressed (dashed lines) Si for two body thicknesses. The mobility components are plotted parallel (closed symbols) and perpendicular (open symbols) to stress direction [001].

Conclusion

The effect of uniaxial stress on the electron mobility was analyzed by means of MC simulations. Experimentally observed mobility data were reproduced for bulk Si and Si inversion layers on (001) and (110) oriented substrates with large and small body thicknesses. Mobility enhancement can be understood only from a combination of three effects: (i) valley (subband ladder) repopulation, (ii) change in inter-valley, inter-subband scattering, and (iii) stress induced effective mass changes. While repopulation effects can increase the bulk and inversion layer mobilities at relatively

large body thicknesses ($T_{\mathrm{SOI}} > 20\,\mathrm{nm}$), the population of higher subband ladders is intrinsically reduced by strong quantum confinement for very small body thickness ($T_{\mathrm{SOI}} < 5\,\mathrm{nm}$). Thus, in the latter case, no mobility enhancement can be expected from stress induced repopulation effects and only the stress induced effective mass change can explain the experimentally observed mobility enhancement. In this aspect, stress conditions reducing the effective mass in transport direction (like uniaxial tensile stress along $\langle 110 \rangle$) are very beneficial to increase mobility in UTB-MOSFETs.

Acknowledgements

This work has been partly supported by the Austrian Science Fund (FWF), projects 17285-N02 and I79-N16.

Bibliography

1. M. V. Fischetti, F. Gamiz, W. Hänsch, *J.Appl.Phys.*, **92**, 7320 (2002).
2. M. V. Fischetti, Z. Ren, *J.Appl.Phys.*, **94**, 1079 (2003).
3. S.-E. Thompson, G. Sun, Y. Choi, T. Nishida, *IEEE Trans.Electron Devices*, **53**, 1010 (2006).
4. J. Bardeen, W. Shockley, *Phys. Rev.*, **80**, 72 (1950).
5. C. Herring, E. Vogt, *Phys. Rev.*, **101**, 944 (1956).
6. K. Uchida, T. Krishnamohan, K. Saraswat, Y.Nishis, in *Proc. Intl. Electron Device Meeting*, 135 (2005).
7. E. Ungersboeck, S. Dhar, G. Karlowatz, H. Kosina, S. Selberherr, in *11th International Workshop on Computational Electronics Book of Abstracts*, 141 (2006).
8. A.-Y. Thean, L. Prabhu, V. Vartanian, M. Ramon, in *Proc. Intl. Electron Device Meeting*, 515 (2005).
9. http://www.iue.tuwien.ac.at/software, VMC 2.0 User's Guide, Institut für Mikroelektronik, Technische Universität Wien, Austria (2006).
10. S. Smirnov, H. Kosina, *Solid-State Electron.*, **48**, 1325 (2004).
11. K. Uchida, J. Koga, S. Takagi, in *Proc. Intl. Electron Device Meeting*, 805 (2003).
12. G. Tsutsui, M. Saitoh, T. Saraya, T. Nagumo, T. Hiramotoy, in *Proc. Intl. Electron Device Meeting*, 747 (2005).
13. R.E. Prange and T.W Nee, *Phys. Rev.*, **168**, 779 (1968).
14. E. Ungersboeck, H. Kosina, in *Proc. Simulation of Semiconductor Processes and Devices*, 311 (2005).
15. H. Irie, K. Kita, K. Kyuno, A. Toriumi, in *Proc. Intl. Electron Device Meeting*, 225 (2004).